NASA
Technical
Paper
2688

May 1987

Quantitative Analysis of the Reconstruction Performance of Interpolants

Donald L. Lansing
and Stephen K. Park

NASA Technical Paper 2688

1987

Quantitative Analysis of the Reconstruction Performance of Interpolants

Donald L. Lansing
Langley Research Center
Hampton, Virginia

Stephen K. Park
The College of William and Mary
Williamsburg, Virginia

National Aeronautics and Space Administration

Scientific and Technical Information Office

Contents

Introduction

Interpolation is a technique of fundamental importance in many disciplines including signal and image processing, computer graphics, computer-aided design (CAD), and numerical analysis. In all these disciplines, one is frequently faced with some version of the following problem: given a discrete set of points which correspond to values of a function $y(x)$ sampled on a grid, construct an easily computed function $g(x)$ which equals $y(x)$ on the sampling grid and approximates $y(x)$ elsewhere. In the signal- and image-processing literature, $g(x)$ is said to *reconstruct* $y(x)$ from its samples; in the computer graphics, CAD, and numerical analysis literature the term *interpolate* is more common. In either case, the concept is the same.

There are numerous interpolation and reconstruction algorithms from which to choose. Most of these algorithms are based upon interpolants which are either polynomial or exponential splines. If the number of samples is small, global algorithms are generally preferred. However, if the number of samples is large, the algorithms are virtually always local. Generally, global splines are used in CAD, graphics, and numerical analysis applications, whereas local splines are employed for signal- and image-processing problems. In either case, choosing an interpolant for a specific application involves a combination of subjective factors including ease of use and the analyst's prior experience and personal judgment as to what constitutes a "good" technique.

This paper is concerned with the application of a quantitative measure of the performance of various interpolation and reconstruction algorithms. The analysis provides a quantitative criterion based upon the mean square error for assessing how well $g(x)$ approximates $y(x)$. It is applicable to the situation commonly occurring in signal- and image-processing in which the number of grid points is very large and the grid is equally spaced. The interpolants under consideration are characterized by the properties of linearity and shift invariance; that is, $g(x)$ is a linear combination of the sample values and a left or right shift of the sample grid produces only a corresponding shift in $g(x)$. The criterion, reformulated in the frequency domain, is applicable to data sets with arbitrary spectral content. However, this paper is primarily concerned with the interpolation of sufficiently sampled, band-limited data. The results provide a unified approach which applies equally well to evaluating interpolants for CAD, graphics, numerical analysis, and image-processing applications.

Symbols

$e^2(\nu)$	function defined by the series in equations (6), expresses an interpolant's contribution to the mean square error
$g(x)$	interpolating function
$H_i(s)$	quintic Hermite basis functions, $i = 1,\ 2,\ 3,\ \ldots,\ 6$
$h_i(s)$	cubic Hermite basis functions, $i = 1,\ 2,\ 3,\ 4$
i, n	knots, sample grid locations
K	integer defining width of interpolation function
$r(x)$	interpolation function
$\hat{r}(\nu)$	reconstruction filter, Fourier transform of $r(x)$
s	$= x - i$, independent variable in Hermite function
x	independent variable of sampled function
$y(n)$	data samples of $y(x)$ at the knots
$y(x)$	function to be sampled and interpolated
$\hat{y}(\nu)$	Fourier transform of $y(x)$
$\lvert\hat{y}(\nu)\rvert^2$	data energy spectrum
$\alpha,\ \beta,\ t,\ t'$	parameters in Hermite interpolation and parametric cubic convolution
ϵ^2	average mean square error
ν	frequency parameter, cycles per sample
ν_c	cut-off frequency
σ	shape parameter in model of data energy spectrum

Abbreviations:

BAWA	piecewise cubic interpolant developed in reference 9
CAD	computer-aided design
PCC	parametric cubic convolution
OBE	unfiltered out-of-band energy

Statement of the Problem

This paper is concerned with the following version of the standard interpolation problem. Suppose that the real-valued function $y(x)$, defined

for all real x, has been sampled at the integers $\ldots, -2, -1, 0, 1, 2, \ldots$ to yield the (noise-free) data $\ldots, y(-1), y(0), y(1), \ldots$. Figure 1 shows several data samples near the nth knot. Construct a computationally efficient interpolating function $g(x)$ for which

1. $g(x) = y(n)$ when $x = n = 0, \pm 1, \pm 2, \ldots$.
2. $g(x)$ is acceptably smooth for all x.
3. $\int_{-\infty}^{\infty} [y(x) - g(x)]^2 \, dx$ is sufficiently small.

Condition (1) forces $g(x)$ to interpolate $y(x)$ at its samples. If this condition were omitted, we would be concerned instead with a version of the standard approximation problem. Condition (2) translates into a statement about the continuity of $g(x)$ and (perhaps) its first and second derivatives. Condition (3) is qualitative; that is, what is "sufficiently small"? We will address this question quantitatively later.

There is no loss of generality in assuming that the domain of $y(x)$ (and thus $g(x)$) is all x. We make this assumption for mathematical convenience; it enables us to ignore the issue of boundary conditions.

There is a significant loss of generality in making the assumption, as is done here, that the sampling grid $(\ldots, -2, -1, 0, 1, 2, \ldots)$ is equally spaced. Certainly for some functions $y(x)$ the only practical way to produce a good interpolating function $g(x)$ is to use an unequally spaced sampling grid. However, there is an important trade-off involved. As discussed in the next section, the assumption of an infinite, equally spaced sampling grid enables us to apply Fourier (i.e., spectral) analysis techniques to this problem and thereby produce valuable insight into how to quantify condition (3).

Many solutions to the interpolation problem are available from the numerical analysis, computer graphics, CAD, and image-processing literature. Among the various types of interpolants commonly used for data analysis and graphics applications are Hermite, cubic, exponential, parabolic, rational, B-, beta-, monotonic, and shape-preserving splines. For a broad, general introduction to spline methods, see reference 1, which contains ready-to-use FORTRAN programs. It is important to distinguish these spline interpolants from the reconstruction algorithms used in image processing. The latter have a central concept—the interpolation function—around which their treatment can be unified. The former, however, are more diverse in their derivations and mathematical representations, and they are rarely, if ever, discussed in terms of their interpolation functions.

The selection of an interpolant is generally a highly subjective matter. The choice involves practical considerations of computational efficiency and subjective evaluations of *fairness*, that is, the visual acceptability of the interpolating function based upon its conformance to the data.

In this paper, condition (3) is used as a criterion to measure the accuracy with which a given interpolating function g reconstructs the original sampled function y. The method by which this quantitative criterion is used to assess the characteristics of interpolants used for data analysis, CAD, and graphics is believed to be new. The criterion is applied to several spline interpolants commonly used in data analysis, CAD, and graphics as well as to several signal and image reconstruction algorithms.

Although the criterion developed encompasses data with arbitrary frequency content, this paper focuses primarily on the interpolation of band-limited and sufficiently sampled data. However, an example of using the data energy spectrum to select an optimal interpolant is presented to indicate how the analysis might be applied to tailor a parametric family of interpolants for best performance with a given class of data.

Analysis

A quantitative analysis of the reconstruction properties of interpolants was derived in reference 2 in an analysis of the effect of sampling and sample-scene phase on image reconstruction. The equations were then applied in reference 3 to study the image reconstruction properties of a particular family of reconstruction algorithms. In this paper, we show that by broadening the interpretation of the basic equations in these two references, it is possible to study many of the interpolants familiar to the numerical analyst and graphics specialist. As a consequence of this expanded interpretation, a unified perspective is achieved which encompasses both signal and image reconstruction algorithms and many of the types of interpolants used for data analysis, CAD, and graphics.

To begin, we present a summary of the underlying equations and concepts from references 2 and 3. The main objective of this presentation is to demonstrate how to reformulate the mean-square-error criterion in a manner which separates the contribution of the particular interpolant being used from the contribution of the data set being analyzed. Subsequently, these equations are applied to a variety of specific interpolants.

Linear, Shift-Invariant Interpolants

The analysis of reference 2 was derived for the class of interpolants that are both linear and shift invariant.[1] Thus, it is important to clearly understand the properties of linear, shift-invariant interpolants.

An interpolant is linear and shift invariant if and only if there exists a function $r(x)$ such that

$$g(x) = \sum_{n=-\infty}^{+\infty} y(n)r(x-n) \qquad (1)$$

Thus, the output function $g(x)$ may be expressed as a linear combination of translated copies of $r(x)$. The function $r(x)$ is called the *interpolation function* for the interpolant. It follows from equation (1) that each interpolant is uniquely defined by its interpolation function $r(x)$ and conversely. For a particular interpolant, $r(x)$ is the (unique) function which interpolates the data ..., 0, 0, 1, 0, 0, ...; that is, the interpolation function $r(x)$ is generated by interpolating this special data set. The interpolation function is fundamental to the quantitative characterization of the reconstruction and interpolatory properties of its associated interpolant. Reconstruction algorithms used for signal and image interpolation are usually expressed directly in terms of an interpolation function. For local, linear, shift-invariant data and graphics splines, the interpolation function can be easily derived in closed form from the defining equations by using these data values.

An interpolant is said to be *local* if there is an integer K such that $r(x) = 0$ whenever $|x| \geq K$. The smallest such integer K defines the width of the interpolation function, and the interpolant is said to be a $2K$-point method. That is, for a local interpolant, the infinite sum in equation (1) reduces to a finite sum since the terms with $|x-n| \geq K$ do not contribute; that is,

$$g(x) = \sum_{n=[x]-K+1}^{[x]+K} y(n)r(x-n)$$

where $[x]$ denotes the greatest integer less than or equal to x. As an example, the interpolation function for linear interpolation is shown in figure 2. Linear interpolation is a local method with $K = 1$. For the other local interpolants considered in this paper, K is either 2 or 3.

[1] Note, however, that some interpolants which appear in the current literature are not linear or shift invariant. An example of a nonlinear spline which is outside the scope of the analysis in this paper is described subsequently.

Data, CAD, and graphics splines are frequently presented in the literature as a linear combination of blending functions with numerical coefficients which are functions of the sample values, for example, Hermite interpolation. However, if the numerical coefficients are *linear* combinations of the sample values, equation (1) provides an alternate and completely equivalent means of carrying out the interpolation. The interpretation of equation (1), shown schematically in figure 3 for linear interpolation, is that the interpolating function, a series of line segments in this example, can be built by convolution, that is, as a sum of *impulse responses*, represented by $r(x-n)$, of amplitude $y(n)$ centered at the samples $x = n$.

Associated with each interpolation function $r(x)$ is its reconstruction filter, that is, Fourier transform $\hat{r}(\nu)$:

$$\hat{r}(\nu) = \int_{-\infty}^{+\infty} r(x)\, e^{-2\pi j x\nu}\, dx \qquad (2)$$

when $j = \sqrt{-1}$. The frequency coordinate ν has the units of cycles per sample interval and $\nu = 1/2$ is the Nyquist frequency. Because all the interpolation functions $r(x)$ considered in this paper are real and even, all the corresponding reconstruction filters $\hat{r}(\nu)$ are also real and even.

Mean-Square-Error Criterion

As discussed previously, we use the mean square error, condition (3),

$$\epsilon^2 = \int_{-\infty}^{+\infty} [y(x) - g(x)]^2\, dx \qquad (3)$$

as the criterion which measures how well an interpolating function g approximates the sampled function y. In reference 2 it was shown that if $y(x)$ is band limited (i.e., the energy spectrum $|\hat{y}(\nu)|^2$ is zero for all $|\nu|$ greater than a cut-off frequency ν_c) and if $y(x)$ is sufficiently sampled (i.e., $\nu_c \leq 1/2$), then equation (3) can be transformed into

$$\epsilon^2 = \int_{-\nu_c}^{+\nu_c} e^2(\nu)|\hat{y}(\nu)|^2\, d\nu \qquad (4)$$

In equation (4),

$$\hat{y}(\nu) = \int_{-\infty}^{+\infty} y(x)\, e^{-2\pi j x\nu}\, dx \qquad (5)$$

is the (complex) Fourier transform of the sampled function $y(x)$ and

$$e^2(\nu) = 1 - 2\hat{r}(\nu) + \sum_{n=-\infty}^{+\infty} \hat{r}^2(\nu - n) \qquad (6a)$$

$$e^2(\nu) = [1 - \hat{r}(\nu)]^2 + \sum_{\substack{n=-\infty \\ n\neq 0}}^{+\infty} \hat{r}^2(\nu - n) \quad (6b)$$

Note that, as the notation suggests, $e^2(\nu)$ is nonnegative for all ν. Also, if the interpolant is a local $2K$-point method, it can be shown that an equivalent equation for $e^2(\nu)$ is

$$e^2(\nu) = 1 - 2\hat{r}(\nu) + c_0 + 2\sum_{n=1}^{2K-1} c_n \cos(2\pi n\nu) \quad (7)$$

where

$$c_n = \int_{n-K}^{K} r(x)r(n-x)\,dx \quad (8)$$

If $y(x)$ is band limited but not sufficiently sampled ($1/2 < \nu_c < \infty$) or if $y(x)$ is not band limited ($\nu_c = \infty$), then the mean square error ϵ^2 depends upon the location of the function $y(x)$ relative to the sampling grid. However, equation (4) remains valid in the sense that it represents the average mean square error over an ensemble of all possible (random, equally likely) shifts of the sampling grid.

Equation (4) expresses the mean square error as an integral of the product of two positive real functions: $e^2(\nu)$ and $|\hat{y}(\nu)|^2$. The function $e^2(\nu)$ represents the contribution of the interpolant, whereas the function $|\hat{y}(\nu)|^2$ represents the contribution of the sampled data. Thus, the choice of interpolant has been separated from the characteristics of the data. Clearly, for a fixed $|\hat{y}(\nu)|^2$, reducing $e^2(\nu)$ reduces the mean square error. In the remainder of this paper, we consider the interrelation among $r(x)$, $\hat{r}(\nu)$, and $e^2(\nu)$ and the potential of minimizing ϵ^2 by reducing $e^2(\nu)$.

Interpolation Methods Investigated

The interpolants considered in this paper can be conveniently grouped into three categories: local splines, global splines, and reconstruction filters. The spline categories consist of several methods suitable for data analysis, CAD, and graphics applications. The reconstruction filters were taken from the signal- and image-processing literature. Although the interpolants selected were chosen to be representative of those which are currently in use or have been studied in recent papers, no attempt was made to exhaustively evaluate all known interpolants. The criterion applied here is proposed only as a suitable means for estimating the quality of an interpolation with linear, shift-invariant interpolants in the context of data analysis or signal or image reconstruction. The results may not be appropriate for evaluating the performance of interpolants for many other uses, such as rendering or display of data, surfacing, or solid modeling.

Background information on the interpolants along with the specifics of their implementation are presented in this section. Several of their salient properties are summarized for quick reference and easy comparison in table I.

Local Splines

As discussed previously, the term *local spline* is used to emphasize the fact that the value of the interpolating function g at a point x depends only upon the values of the $2K$ data samples closest to x. With the exception of these $2K$ samples, the value of the interpolant at x is independent of the data. For both local splines considered, $K = 2$, and thus only the four nearest sample values contribute to the interpolated value.

Parametric cubic Hermite splines. A three-parameter, four-point family of local cubic splines with a Hermite basis was introduced in reference 4 for the purpose of generating "in-between" frames from key frames for an automated animation system. The three parameters, referred to as "tension," "continuity," and "bias," facilitate control of the spline shape and enable the user to generate desired animation effects. For our purposes, we have chosen to set the continuity and bias parameters to zero because our experience indicated that nonzero values tend to produce distortions unsuitable for data interpolation. Therefore, only the tension parameter, assumed constant for the entire spline (to make the spline shift invariant), is used to shape the spline. The equations for the resulting one-parameter family of shift-invariant C^1 splines are given in appendix A. It can be seen from these equations that the tension parameter t or equivalently the parameter $\alpha = -(1-t)/2$, adjusts the values of the spline slopes at the end points of the interval containing the point x at which an interpolation is desired. From this observation, it is clear that although α is unconstrained; values of α much outside the range from -1 to $+1$ generally introduce undesirable slopes in $g(x)$ at the sample points. When $\alpha = -1/2$, one obtains the Catmull-Rom spline for which

$$D(i) = \frac{y(i+1) - y(i-1)}{2} = \frac{y(i) - y(i-1)}{2} + \frac{y(i+1) - y(i)}{2}$$

That is, the slope assigned at the point i is the average of the slopes of the left-hand chord $y(i) - y(i-1)$ and right-hand chord $y(i+1) - y(i)$.

Parametric quintic Hermite splines. The one-parameter subclass of cubic Hermite splines above is identical, except for minor notational changes, to a one-parameter family of cubic splines developed independently by Fletcher and McAllister.[2] These splines are viewed as data interpolants and are generalized in two ways: (1) to two dimensions for generating interpolating surfaces and (2) to higher degree. Our interest is in this latter extension which gives a two-parameter family of fifth degree polynomials. The equations for this four-point, local spline are given in appendix A. The quintic Hermite basis functions $H_1(x)$ to $H_6(x)$ are used; $D(i)$ and $D(i+1)$ are the slopes at the ends of the interval containing the interpolated point; $C(i)$ and $C(i+1)$ are the second derivatives. The two parameters t and t' are referred to as "tension" parameters by Fletcher and McAllister. These parameters control the shape of the interpolant. It can be seen from equations (A5) and (A6) that t, or equivalently $\alpha = -(1-t)/2$, is a weighting factor for slope control, whereas t', or equivalently $\beta = -(1-t')/2$, weights the second derivative terms. In this paper α and β are assumed constant for the entire spline, thus producing a shift-invariant C^2 interpolant. As with the cubic Hermite splines, values of α and β out of the range from -1 to $+1$ introduce undesirable slope and curvature terms with consequent distortion in the interpolating spline.

Global Splines

Global splines are fundamentally different from local splines in that the value of the interpolating function at any point depends upon *all* the data samples. A system of linear algebraic equations must be solved in order to construct the interpolant. Because of this additional computational effort these interpolants are generally used only with relatively small data sets.

Exponential splines. The exponential spline in tension (refs. 5 and 6) is a popular form of global spline. The tension parameter provides control over the spline shape, and the well-known cubic spline is obtained as a limiting case of the exponential spline with zero tension. Exponential splines are commonly used to eliminate the extraneous oscillations which are frequently obtained with cubic splines. However, exponential splines cannot be evaluated quite as efficiently as cubic splines, and this has been cited as a potential drawback in time-critical applications.

[2] Fletcher, G. Yates; and McAllister, David F.: A Unified Approach to Cardinal Spline Surfaces. Unpublished research, North Carolina State Univ., under NASA grant NAG1-103-S4.

The construction of an exponential spline requires the solution of a tri-diagonal system of linear equations which account for the interaction of all the data points. The algorithm used in this paper for calculating exponential splines is based on the equations of reference 6. The tension parameter, designated p in reference 6, is held constant along the length of the spline in order to preserve shift invariance.

Nu splines. The nu spline (ref. 7) was developed as a piecewise cubic polynomial alternative to the exponential spline in tension. This spline is not as computationally expensive as exponential splines since polynomial functions are involved. Nu splines may be generated by using the cubic Hermite basis functions in appendix A. The values of the unknown slopes at the samples are determined by solving a tri-diagonal system of equations which express continuity conditions along the spline. For this study, the tension parameter, denoted ν in reference 7, is constant along the curve resulting in a C^2 shift-invariant interpolant. As in the case of the exponential spline, zero tension corresponds to the cubic spline.

Global interpolation functions. Local splines possess spatially limited interpolation functions $r(x)$ whose translation invariance is usually clear from the equations defining the spline. The situation is quite different for global splines. To generate a global spline, one must solve a set of linear equations which represent an interaction between all the data values and the end conditions. As a result, an interpolated value depends upon the end conditions and all the sample values, not just upon the values of a few neighboring samples. Consequently, global splines do not have interpolation functions in the same sense as local splines. The function which interpolates the data ..., 0, 0, 1, 0, 0, ... depends upon the location of the unit value relative to the end points (i.e., it is not shift invariant), the number of samples, and the end conditions. Moreover, the interpolation function (theoretically) never becomes identically zero.

Nevertheless, we have verified by numerical experimentation using from 25 to 100 knots that for both exponential and nu splines, interpolation functions can be generated which are shift invariant well within plotting accuracy (generally, 3–5 significant figures) except when centered at a few samples (4–5) near the ends. Therefore, as an excellent *approximation* for global interpolants one can define a surrogate interpolation function which exhibits the essential features of locality and shift invariance and plays a role equivalent to the interpolation function for a local spline. This function can be calculated in the same manner as for a local spline provided that the unit

value is not placed too close to an end sample and a sufficient number of samples (25 or more) are taken. Equation (1) and the subsequent analysis are then applicable in a generalized sense, and in this way, we are able to include exponential, cubic, and nu splines in this study. Because global splines are frequently used for curve fitting and data analysis, it is highly desirable to establish some basis for comparing their reconstruction properties with those of local splines.

Reconstruction Filters

Considerable effort has been expended in developing efficient and accurate algorithms for interpolating and resampling digital signals and images. Since the analysis applied here was originally developed in an image-processing context, it is natural to include several such algorithms in our comparison. These algorithms are specified directly in terms of their interpolation functions, which are given in appendix B.

Parametric cubic convolution (PCC). PCC is a local, four-point interpolant whose interpolation function is given by a one-parameter family of piecewise cubic polynomials (eqs. (B2) through (B4)). The original analysis of reference 2 was applied to this interpolant in reference 3 in order to choose an optimal value of the parameter α. It was demonstrated that if the energy spectrum of the image could be estimated, it is possible to choose the parameter to optimize the reconstruction properties so as to take this spectrum into account. However, for general purpose use, that is, in the absence of specific information regarding the frequency content of the image, $\alpha = -1/2$ was found to be the optimum value from the standpoint of minimizing the mean square error, provided that the data are sufficiently sampled. This choice of α was not the value generally referenced in the literature and resulted in a reconstruction algorithm generally superior to the prevailing standard.

As indicated in appendix B, the equations for the PCC interpolation function are identical to those for parametric cubic Hermite splines. Thus, these two interpolants are identical. This equivalence does not appear to have been observed before and illustrates an advantage to having a unified treatment of interpolants.

Keys' cubic. Keys' cubic is a local, six-point interpolant whose interpolation function is again given by piecewise cubic polynomials. However, in contrast to PCC, there are no free parameters. The algorithm is fourth order convergent (ref. 8) which is the highest order which can be achieved with cubic polynomials; and therefore, it is expected that this algorithm will perform somewhat better than PCC with $\alpha = -1/2$. However, because this is a six-point interpolant, any improvement in performance is achieved at some additional computational expense.

BAWA cubic. Two 4-point interpolants based on piecewise cubic polynomials are presented in reference 9. In reference 9, the interpolant whose interpolation function is denoted by $a_1(t)$ is identical to PCC with $\alpha = -1/2$. The other interpolant is defined by a continuous interpolation function with a discontinuous first derivative at the sample points 0, ± 1, ± 2, a very novel feature. As illustrated in reference 9, the associated reconstruction filter has a slightly more band-limited spectrum than PCC with $\alpha = -1/2$. This second interpolant has been included in our comparison.

Quadratic Shape-Preserving Splines

Because not all local splines are both linear and shift invariant, some local interpolants do not fall within the scope of the current analysis. For example, parametric cubic and quintic splines lose the property of shift invariance if their parameters are allowed to vary from one sample interval to the next. As the following example illustrates, some interpolants can also fall outside the scope of the current analysis by failing to be linear.

The second-degree polynomial "shape-preserving" splines described in reference 10 were introduced in an effort to preserve the monotonicity and convexity suggested by a visual inspection of the data. By introducing at most one variable knot between samples, a quadratic spline is produced which interpolates the data and preserves shape. This interpolant depends upon certain shape characteristics of second-degree Bernstein polynomials and the specification of appropriate slopes at the knots. The resulting spline is C^1. These splines have also been suggested (ref. 11) for shape-preserving interpolation of bivariate functions on rectangular grids. The examples in references 10 and 11 show very smooth interpolating functions and surfaces free of unwanted wrinkles. There are no variable parameters for controlling shape.

The nonlinearity of this spline arises if the method suggested in reference 10 is employed to assign slopes at the knots. These slopes $M(i)$ are defined so as to ensure that the monotonicity and convexity of the data are preserved and are calculated in the following manner. At knot i, let $S(i) = y(i) - y(i-1)$ and $S(i+1) = y(i+1) - y(i)$ be the slopes of the

left-hand and right-hand chords, respectively. Then

$$M(i) = \begin{cases} 0 & (S(i)S(i+1) \leq 0) \\ \frac{2S(i)S(i+1)}{S(i)+S(i+1)} & (\text{Otherwise}) \end{cases}$$

Although the $M(i)$'s enter into the definition of the spline in a linear manner, they depend upon the sample values in a highly nonlinear fashion. The spline is local since only four sample points are used in an interpolation. However, the resulting spline cannot be represented by equation (1), and thus, the subsequent analysis does not apply.

Comparison of Reconstruction Properties of Interpolants

In this section, plots of $r(x)$, $\hat{r}(\nu)$, and $e(\nu)$ are presented for the interpolants described previously. Examination of the interpolation function $r(x)$ and the reconstruction filter, $\hat{r}(\nu)$ provides a qualitative indication of the performance of an interpolant. In contrast, because of equation (4), the $e^2(\nu)$ function provides more quantitative information. That is, by comparing $e(\nu)$ functions, judgments can be made regarding the minimization of the mean square error by the proper choice of interpolant.

For the data and graphics splines, values of $r(x)$ were generated numerically using a 101-point data set (100 sample intervals each of unit length) with 1 for the middle (51st) data value and all zeros otherwise. For the global interpolants, the tridiagonal systems of linear equations given in references 6 and 7 had to be solved. For the local splines, the defining equations given in appendix A were used; and for the reconstruction filters, the equations in appendix B. For each interpolant, the reconstruction filter $\hat{r}(\nu)$ was calculated with a fast Fourier transform (FFT) routine using 4096 values of $r(x)$ taken over an interval that was 100 sample intervals in length. Because $r(x)$ is a real, even function of $x, \hat{r}(\nu)$ is a real, even function of ν. Values of the reconstruction filter are therefore available for negative ν by symmetry. Thus, values of $\hat{r}(\nu)$ have been calculated in steps of 0.01 from $\nu = -20.47$ to $\nu = +20.47$. For $|\nu| \geq 20.48$, it is assumed that $\hat{r}(\nu) = 0$. From equations (6) or (7), it may be seen that $e^2(\nu)$ is an even function of ν. For positive ν, $e^2(\nu)$ was calculated directly from equation (6) with the infinite series truncated when $|\nu - n| \geq 20.48$.

As an aid in interpreting the results presented herein, it is helpful to recall (ref. 12) that if $y(x)$ is band limited and sufficiently sampled, then it can be reconstructed *exactly* by using the "ideal" interpolation function,

$$r(x) = \frac{\sin(\pi x)}{\pi x}$$

for which

$$\hat{r}(\nu) = \begin{cases} 1 & (|\nu| < 0.5) \\ 0 & (0.5 < |\nu|) \end{cases}$$

and

$$e^2(\nu) = \begin{cases} 0 & (|\nu| < 0.5) \\ 2 & (0.5 < |\nu|) \end{cases}$$

as shown in figure 4.

This reconstruction filter is ideal in the sense that if $y(x)$ is band limited and sufficiently sampled, then the mean square error ϵ^2 is zero since $e^2(\nu) = 0$ for $0 \leq \nu \leq 0.5$ and $|\hat{y}(\nu)|^2 = 0$ for $|\nu| > 0.5$. However, this reconstruction technique cannot be used as the basis of a practical interpolation method because of the infinite domain of $r(x)$.

The ideal reconstruction filter defines the desirable characteristics of a practical interpolant to use with band limited and sufficiently sampled data: an $\hat{r}(\nu)$ which is as flat as possible at unit value for $\nu \leq 0.5$ and drops rapidly to 0 for $\nu \geq 0.5$. Or equivalently, an $e^2(\nu)$ which is as small as possible throughout the range $0 \leq \nu \leq 0.5$. The latter is a quantitative criterion coming directly from equation (4).

Interpolation Function

The interpolation function $r(x)$ for several of the interpolants investigated is shown in figure 5. The heavy dots in figure 5 mark the locations of the knots. The interpolation functions are all even functions of x which take on the special values $r(0) = 1$ and $r(\pm n) = 0$ for $n = 1, 2, 3, \ldots$. The functions have been separated vertically in the figure to facilitate comparison.

A few features deserve mention. The persistent oscillation of the ideal interpolant for many sample intervals is indicated. The discontinuity in slope of the BAWA cubic at the knots is evident. Also, of the interpolants studied, the cubic spline has the widest interpolation function with an effective K of 5; that is, for $|x| > 5$, $|r(x)| \leq 0.001$. As the tension is increased from 0 to 50, $r(x)$ for the exponential spline changes from that of the cubic spline to nearly triangular shape which characterizes linear interpolation.

Figure 6 shows how the shape of $r(x)$ varies with α for parametric cubic and quintic Hermite interpolation. Recall that α is the slope of $r(x)$ at $x = 1.0$ and note that figure 6(a) also applies to

PCC. Figures 6(a) and 6(b) are quite similar. The parameter β permits further fine-tuning of the shape of $r(x)$ if desired for quintic Hermite interpolation.

Reconstruction Filter

Figure 7 presents plots of $|\hat{r}(\nu)|$ on the range $0 \leq \nu \leq 2.0$ for selected interpolants. Keys' cubic (fig. 7(a)), which has the highest order convergence that can be obtained with piecewise cubic polynomials, exemplifies the ideal features of a reconstruction filter: flat near $\nu = 0$, rapid drop to zero near $\nu = 1/2$, and only a very weak sideband peaking near $\nu = 1.5$.

The reconstruction filter for PCC with $\alpha = -1/2$ (fig. 7(b)) begins to roll off from 1.0 at slightly smaller values of ν than does Keys' cubic and has a somewhat more gradual decline to 0. There are two weak sidebands between 1.0 and 2.0. However, recall that PCC uses fewer sample values than Keys' cubic and is therefore a more computationally efficient interpolant.

The reconstruction filter for the BAWA cubic (fig. 7(c)) is not as ideal as that for Keys' cubic. However, it is quite similar to PCC with $\alpha = -1/2$ in the range $\nu \leq 1.0$ where it has a somewhat narrower spectrum. Note, however, the significant, undesirable sideband at $\nu = 1.5$.

Of all the interpolants analyzed, the cubic spline displays the best performance for sufficiently sampled data as judged by the shape of its reconstruction filter. As can be seen from figure 7(d), the reconstruction filter for the cubic spline is very flat at $\nu = 0$ and drops abruptly to zero just beyond $\nu = 1/2$. Thus, the cubic spline has ideal reconstruction characteristics superior to both Keys' cubic and PCC. However, because it is a global interpolant, it is considerably more computationally intensive than local methods, and it is not suitable for reconstructing large amounts of data.

Figures 7(e) and 7(f) show the reconstruction filters for two global interpolants. Tightening an exponential spline (fig. 7(e)), by adding tension (0 tension gives the cubic spline) causes the flat section at $\nu = 0$ to be rounded off and a prominent sideband to appear above $\nu = 1.0$. These are both undesirable features. (As a point of reference, Tension = 50 for the exponential spline generates nearly linear interpolation.) Tensioning a nu spline (fig. 7(f)) produces similar effects.

In summary, of all the interpolants analyzed, the one whose reconstruction filter is closest to ideal is the cubic spline followed by Keys' cubic and then the BAWA cubic and PCC with $\alpha = -1/2$. Since the cubic spline is a limiting case of the exponential and nu splines with 0 tension, there is a small range of values of tension just above 0 for which these global interpolants also produce more ideal response than the local methods.

The Function $e^2(\nu)$

The function $e^2(\nu)$ appears as part of the integrand in the spectral representation of the mean square error (eq. (4)). Hence, the shape of $e^2(\nu)$ has a direct quantitative influence upon the reconstruction performance of an interpolant. Judgments can be made regarding the relative mean square error of several interpolants and the interpolant with the least mean square error may be identified by comparing $e^2(\nu)$ functions. Closed form expressions for $e^2(\nu)$ for linear interpolation (highly tensioned splines), PCC, and the BAWA cubic are given in appendix C.

Figure 8 shows plots on a linear scale of four typical $e^2(\nu)$ functions on the range $0 \leq \nu \leq 2.0$. Recall that $e^2(\nu)$ is an even function of ν. The curves are very flat near $\nu = 0$ but rise rapidly to a relative maximum of about 2.0 near $\nu = 1$. The $e^2(\nu)$ function is almost periodic for large ν as can be deduced directly from equation (6); that is, as $|\nu| \rightarrow +\infty$, $|\hat{r}(\nu)| \rightarrow 0$ and the remaining terms in equation (6) represent a periodic function with period 1.

Figure 9 is a composite plot of $e(\nu)$ for several interpolants on a semilogarithmic scale for ν below the Nyquist frequency. This is the range of ν which contains the significant energy for an adequately sampled data set and normally is the only portion of the range of integration in equation (4) which makes a substantial contribution to the average mean square error. Observe from equation (4) that for a given data energy spectrum $|\hat{y}(\nu)|^2$, the average mean square error is minimized by the interpolant having the smallest $e^2(\nu)$ over this range of ν.

Referring to figure 9, it is again evident that the cubic spline is the best choice of all the interpolants analyzed. Keys' cubic is the best of the local methods. The BAWA cubic and PCC with $\alpha = -1/2$ are next in line among the local methods. Adding tension to either the nu or the exponential spline raises the ordinates of the $e(\nu)$ curve and hence degrades the spline's performance. Small tensions, roughly up to about 2.0, result in small deviations from the cubic spline. Hence, there is a range of tension for which the nu and exponential splines perform better, but at greater computational cost, than the local methods. This examination of the $e(\nu)$ function reconfirms the conclusions reached by the previous comparison of the reconstruction filters.

Optimized Quintic Hermite Splines

Parametric quintic Hermite interpolation has two

parameters, α and β. It is of interest to try to select these parameters so as to optimize the reconstruction performance of this interpolant. In reference 3, it was observed that the superior performance of PCC with $\alpha = -1/2$ manifests itself in two ways: the reconstruction filter and the $e^2(\nu)$ function are both very flat near $\nu = 0$. Specifically, the Taylor series expansions of these functions have the form $\hat{r}(\nu) = 1.0 + O(\nu^4)$ and $e^2(\nu) = O(\nu^6)$ for small ν. The results of selecting α and β so as to duplicate this behavior for quintic Hermite splines are briefly discussed in this section.

First, consider choosing the parameters to make $\hat{r}(\nu)$ flat at $\nu = 0$. The Taylor series expansion of $\hat{r}(\nu)$ in powers of ν was generated from equations (2) and (B6) through (B9) using a software package for symbolic manipulation. The coefficients of the ν^2 and ν^4 terms were then set to zero in order to remove the low order terms from the expansion. This resulted in two equations for α and β with the solution $\alpha = 117/32$ and $\beta = 37$. The functions $\hat{r}(\nu)$ and $e(\nu)$ for these values of α and β are shown in figure 10. While $\hat{r}(\nu)$ is indeed very flat at $\nu = 0$, the drop to zero at $\nu = 1.0$ is delayed to well above the Nyquist frequency and a very large sideband becomes evident. The $e(\nu)$ function is clearly inferior to any seen in previous sections. In other words, in this case the "design criteria" of choosing the interpolant parameters to flatten $\hat{r}(\nu)$ near $\nu = 0$ was a bad idea.

Next, an effort was made to choose α and β to make $e^2(\nu)$ flat near $\nu = 0$. The Taylor series expansion of $e^2(\nu)$ in powers of ν was found up to ν^6 and then the coefficients of the ν^2 and ν^4 terms were set to zero and solved for α and β giving $\alpha = -1/2$ and $\beta = -1$. The functions $\hat{r}(\nu)$ and $e(\nu)$ are shown in figure 11. These results produce a spline which is certainly quite acceptable for application; that is, the design criteria of choosing the interpolant parameters to flatten $e^2(\nu)$ near $\nu = 0$ proved to be a good idea. However, when figure 11(b) and figure 9 are carefully plotted on the same scale, it can be seen that, while the $e(\nu)$ function is close to that for PCC with $\alpha = -1/2$ and that for the BAWA cubic, it is actually somewhat above both of these curves. Therefore, the optimized quintic Hermite spline is not quite as good for minimizing the mean square error as either PCC with $\alpha = -1/2$ or the BAWA cubic.

In conclusion, attempts to optimize the reconstruction performance of parametric quintic Hermite interpolants by choosing α and β to render $\hat{r}(\nu)$ and $e^2(\nu)$ flat near $\nu = 0$ have not led to an improved interpolant. These negative results highlight the need to employ more sophisticated optimization criteria in order to obtain useful results.

Optimized Parametric Cubic Interpolants

In the previous section, an attempt was made to optimize the performance of a parametric family of interpolants by choosing the parameters to mimic the spectral characteristics of the ideal interpolant. In this section, we demonstrate that a more comprehensive optimization of a family of interpolants may be performed if $|\hat{y}(\nu)|^2$ is known. Specifically, we illustrate how PCC can be optimized using an assumed model for the data energy spectrum. This example illustrates how the theoretical foundation laid earlier in the paper may be used to select the parameters in a family of interpolants to produce the best reconstruction performance.

Using equation (4) and equation (C7) for $e^2(\nu)$ for PCC, it can be shown that for data with energy spectrum $|\hat{y}(\nu)|^2$, the average mean square error of the interpolation is

$$\epsilon^2 = \int_{-\nu_c}^{+\nu_c} e_0(\nu)|\hat{y}(\nu)|^2\,d\nu - 2\alpha\int_{-\nu_c}^{+\nu_c} e_1(\nu)|\hat{y}(\nu)|^2\,d\nu + \alpha^2\int_{-\nu_c}^{+\nu_c} e_2(\nu)|\hat{y}(\nu)|^2\,d\nu \tag{9}$$

where e_0, e_1, and e_2 are defined in equation (C8) and where ν_c may be ∞ (if the data are not band limited).

The mean square error is minimum when $d\epsilon^2/d\alpha = 0$, that is, when

$$\alpha = \alpha_{\text{opt}} = \frac{\int_{-\nu_c}^{+\nu_c} e_1(\nu)|\hat{y}(\nu)|^2\,d\nu}{\int_{-\nu_c}^{+\nu_c} e_2(\nu)|\hat{y}(\nu)|^2\,d\nu} \tag{10}$$

The existence of a minimum is assured since the coefficient of α^2 in equation (9) is positive. Thus, the mean square error when using parametric cubic convolution or parametric cubic Hermite splines is least when $\alpha = \alpha_{\text{opt}}$. As shown in reference 3, $e_1(\nu)$ is negative below the Nyquist frequency. Hence, α_{opt} is negative for sufficiently sampled data.

To model the data energy spectrum, we assume the model

$$|\hat{y}(\nu)|^2 = \frac{2\sigma}{1 + (2\pi\sigma\nu)^2} \tag{11}$$

The spectrum, sketched in figure 12, peaks (at a value of 2σ) at $\nu = 0$, then rolls off, and steadily decreases to 0 as $\nu \to \infty$ so as to represent in an ideal way the decay of higher spatial frequencies to be expected in a typical data energy spectrum. The parameter σ controls the rate of decay of the higher harmonics and the peakedness of the spectrum. For convenience, the

total energy in the spectrum has been normalized to unity:

$$\int_{-\infty}^{+\infty} |\hat{y}(\nu)|^2 \, d\nu = 1$$

The *unfiltered* out-of-band energy (OBE) for any data energy spectrum is defined to be the energy beyond the Nyquist frequency:

$$\text{OBE} = \int_{-\infty}^{-1/2} |\hat{y}(\nu)|^2 \, d\nu + \int_{1/2}^{+\infty} |\hat{y}(\nu)|^2 \, d\nu$$

For the spectrum in equation (11),

$$\text{OBE} = 1 - \frac{2}{\pi} \tan^{-1}(\pi\sigma)$$

As indicated in figure 12, the OBE measures the fraction of energy under that part of the spectrum associated with aliasing; large values of OBE are associated with significant aliasing. Instead of using the explicit parameter σ, the implicit parameter OBE is used as the independent variable in subsequent plots and calculations. The corresponding value of σ is

$$\sigma = \frac{1}{\pi} \tan\left[\frac{\pi}{2}(1 - \text{OBE})\right] = \frac{1}{\pi \cot\left(\frac{\pi}{2}\text{OBE}\right)} \qquad (12)$$

The spectral model in equation (11) exhibits a long, slowly decaying tail at high frequencies. In practice, much of this tail would have been effectively removed by appropriate low-pass filtering. We allow for that in our spectral model by incorporating a function to simulate such low-pass filtering. Specifically, we assume a three-pole low-pass Butterworth filter with its effective cut-off set to the Nyquist frequency. Our final spectral model, which includes filtering, is then

$$|\hat{y}(\nu)|^2 = \frac{2\sigma}{1 + (2\pi\sigma\nu)^2} \left[\frac{1}{1 + (2\nu)^6}\right] \qquad (13)$$

The optimal value of α for PCC for this data energy spectrum may be calculated from equations (10) and (13). In theory, one must set $\nu_c = \infty$ to account for the aliased part of the data spectrum. In practice, $\nu_c = 2$ is adequate because of the rapid decay of equation (13) at high frequencies. Equation (12) is used to determine the value of σ corresponding to a given value of *unfiltered* OBE.

The results are shown in figure 13 which presents a plot of α_{opt} for out-of-band energies up to 10 percent (OBE = 0.10). The optimum α is negative over most of the range and generally somewhat less than the value of -0.5 which is optimum for sufficiently sampled (no aliasing) data. A value of -0.7 would be an appropriate average to use over the upper 60 percent of the range of OBE shown.

It is of interest to compare the absolute mean square errors for several of the interpolants studied using the spectral model in equation (13). For each, the average mean square error has been calculated directly from equation (4). The results are shown in figure 14 which is a logarithmic plot of ϵ^2 versus unfiltered OBE. The curve for linear interpolation also represents the results for highly tensioned nu and exponential splines. The relative magnitude of the mean square errors is seen to be consistent with the conclusions drawn earlier in the paper regarding the ranking of various interpolants in terms of their reconstruction performance. That is, the mean square error is highest for highly tensioned splines, lowest for the cubic spline, with the other interpolants falling in between in order as expected. The curve for the BAWA cubic is indistinguishable from that for PCC with $\alpha = -1/2$ to the scale used in the plot. Actually ϵ^2 for the BAWA is approximately 1 percent higher than that for PCC because $e^2(\nu)$ for BAWA is slightly larger than $e^2(\nu)$ for PCC for $\nu \geq 0.4$, indicating a very slight preference for PCC. It is interesting to observe that the calculated results in figure 14 fall on virtually straight parallel lines over the range shown implying a relation of the form $\epsilon^2 = A(\text{OBE})^B$ in which A depends on the interpolant but B does not.

Again, recall that PCC, cubic Hermite, and BAWA are local four-point interpolants which are somewhat more computationally efficient than Keys' six-point cubic and are much more computationally efficient than the cubic spline. For the spectral model used, these four-point interpolants would be very attractive since their mean square errors are only slightly larger than those for the more computationally demanding Keys' and cubic interpolants.

Concluding Remarks

An analysis has been presented which provides a quantitative measure of the reconstruction or interpolation performance of linear, shift-invariant interpolants. The performance criterion is the mean square error of the difference between the sampled and reconstructed functions. The analysis is applicable to reconstruction algorithms used in signal and image processing and to many of the types of splines used in numerical analysis, computer-aided design (CAD), and computer graphics. When formulated in the frequency domain, the mean square error clearly separates the contribution of the interpolation method from the contribution of the

sampled function and provides a rational basis for selecting an "optimal" interpolant; that is, one which minimizes the mean square error. Several examples of optimized interpolants are presented.

The analysis has been applied to a collection of frequently used reconstruction and interpolation techniques: parametric cubic and quintic Hermite splines, exponential and nu splines (including the special case of the cubic spline), parametric cubic convolution, Keys' fourth-order cubic, and a cubic with a discontinuous first derivative (the BAWA cubic). The performance of these techniques has been analyzed in the case in which no a priori knowledge of the frequency spectrum of the sampled function is assumed and in one specific case where the spectrum is assumed known.

It has been found that with the proper identification of parameters, interpolation with parametric cubic Hermite splines, developed for computer graphics and curve-fitting applications, is identical to reconstruction with parametric cubic convolution (PCC), a family of reconstruction algorithms used for signal and image processing. Of all the interpolants investigated, it was found that the cubic spline provides the best performance. Adding tension to a cubic spline in the form of either an exponential or nu spline, generally increases the mean square error. Fifth degree Hermite splines showed no advantage over third degree Hermite splines. However, parametric quintic splines possess two parameters which might be selected to tailor an optimal interpolant for a specific application. Of the reconstruction algorithms studied, Keys' cubic exhibited the best performance, as expected, followed by the very similar BAWA cubic with a discontinuous first derivative and cubic Hermite or PCC with $\alpha = -1/2$.

In practical application, these conclusions must be weighed against the computational expense. Cubic, nu, and exponential splines are global interpolants requiring the solution of systems of linear equations. Their use with large data sets demands considerably more computational resources than the local methods—PCC, Keys' cubic, and BAWA cubic. Even the choice of Keys' cubic, which requires six samples, in preference to BAWA cubic or PCC, which require only four samples, would have to be carefully considered for general purpose application to high-resolution images because of the additional computation.

NASA Langley Research Center
Hampton, VA 23665-5225
March 4, 1987

Appendix A

Equations for Hermite Basis Splines

This appendix presents the equations for calculating the interpolating function $g(x)$ for cubic and quintic Hermite splines. In the discussion that follows, suppose x lies between i and $i+1$ and define $s = x - i$.

Parametric Cubic Hermite Splines

The equation for the interpolating function is

$$g(x) = y(i)h_1(s) + y(i+1)h_2(s) + D(i)h_3(s) + D(i+1)h_4(s) \tag{A1}$$

where

$$D(i) = \alpha[y(i-1) - y(i+1)] \tag{A2}$$

and $\alpha = -(1-t)/2$ where t is the tension parameter used in reference 4. The functions $h_i(s)$ are the standard cubic Hermite basis functions defined as

$$\left.\begin{aligned} h_1(s) &= s^2(2s-3)+1 \\ h_2(s) &= s^2(3-2s) \\ h_3(s) &= s^2(s-2)+s \\ h_4(s) &= s^2(s-1) \end{aligned}\right\} \tag{A3}$$

The $h_i(s)$ are defined such that $g(i) = y(i)$, $g'(i) = D(i)$, $g(i+1) = y(i+1)$, and $g'(i+1) = D(i+1)$. Thus the parameter α weights the slopes of the interpolating function g at the end points i and $i+1$, and the four neighboring data points $y(i-1)$, $y(i)$, $y(i+1)$, and $y(i+2)$ contribute to the value of $g(x)$.

Parametric Quintic Hermite Splines

The equation for the interpolating function is

$$g(x) = y(i)H_1(s) + y(i+1)H_2(s) + D(i)H_3(s) + D(i+1)H_4(s) + C(i)H_5(s) + C(i+1)H_6(s) \tag{A4}$$

where

$$D(i) = \alpha[y(i-1) - y(i+1)] \tag{A5}$$

$$C(i) = -\beta[y(i-1) - 2y(i) + y(i+1)] \tag{A6}$$

and $\alpha = -(1-t)/2$ and $\beta = -(1-t')/2$ where t and t' are the two tension parameters.

The functions $H_i(s)$ are the quintic Hermite basis functions:

$$\left.\begin{aligned} H_1(s) &= 1 - s^3(6s^2 - 15s + 10) \\ H_2(s) &= s^3(6s^2 - 15s + 10) \\ H_3(s) &= s - s^3(3s^2 - 8s + 6) \\ H_4(s) &= -s^3(3s^2 - 7s + 4) \\ H_5(s) &= -s^2(s^3 - 3s^2 + 3s - 1)/2 \\ H_6(s) &= s^3(s^2 - 2s + 1)/2 \end{aligned}\right\} \tag{A7}$$

It is easily verified that $g(i) = y(i)$, $g'(i) = D(i)$, and $g''(i) = C(i)$. Thus, α weights the slopes of g at the ends of the interval, and β weights the second derivatives. Again, only four data points, $y(i-1)$, $y(i)$, $y(i+1)$, and $y(i+2)$, enter into the definition of g.

Appendix B

Interpolation Functions

This appendix presents the equations for the interpolation functions for the local splines and the reconstruction algorithms. The functions $h_i(x)$ $(i = 1, 2, 3, 4)$ and $H_i(x)$ $(i = 1, 2, \ldots, 6)$ are the cubic and quintic Hermite basis functions defined in appendix A. The equations for the interpolation functions are as follows:

Parametric cubic convolution

$$r(x) = \begin{cases} -\alpha h_4(x+2) & (-2 \le \times \le -1) \\ h_2(x+1) - \alpha h_3(x+1) & (-1 \le x \le 0) \\ h_1(x) + \alpha h_4(x) & (0 \le x \le +1) \\ \alpha h_3(x-1) & (+1 \le x \le +2) \\ 0 & (2 \le |x|) \end{cases} \tag{B1}$$

$$= r_0(x) + \alpha r_1(x) \tag{B2}$$

where

$$r_0(x) = \begin{cases} (2|x|+1)(|x|-1)^2 & (0 \le |x| \le +1) \\ 0 & (+1 \le |x|) \end{cases} \tag{B3}$$

$$r_1(x) = \begin{cases} |x|vert^2(|x|-1) & (0 \le |x| \le 1) \\ (|x|-1)(|x|-2)^2 & (1 \le |x| \le 2) \\ 0 & (2 \le |x|) \end{cases} \tag{B4}$$

Parametric cubic Hermite splines

The equations are the same as equations (B2) through (B4).

Parametric quintic Hermite splines

$$r(x) = \begin{cases} -\alpha H_4(x+2) - \beta H_6(x+2) & (-2 \le x \le -1) \\ H_2(x+1) - \alpha H_3(x+1) - \beta H_5(x+1) + 2\beta H_6(x+1) & (-1 \le x \le 0) \\ H_1(x) + \alpha H_4(x) + 2\beta H_5(x) - \beta H_6(x) & (0 \le x \le 1) \\ \alpha H_3(x-1) - \beta H_5(x-1) & (1 \le x \le 2) \\ 0 & (2 \le |x|) \end{cases} \tag{B5}$$

$$= r_0(x) + \alpha r_1(x) + \beta r_2(x) \tag{B6}$$

where

$$r_0(x) = \begin{cases} -6|x|^5 + 15|x|^4 - 10|x|^3 + 1 & (0 \le |x| \le 1) \\ 0 & (1 \le |x|) \end{cases} \tag{B7}$$

$$r_1(x) = \begin{cases} -3|x|^5 + 7|x|^4 - 4|x|^3 & (0 \le |x| \le 1) \\ -3|x|^5 + 23|x|^4 - 68|x|^3 + 96|x|^2 - 64|x| + 16 & (1 \le |x| \le 2) \\ 0 & (2 \le |x|) \end{cases} \tag{B8}$$

$$r_2(x) = \begin{cases} -\frac{3}{2}|x|^5 + 4|x|^4 - \frac{7}{2}|x|^3 + |x|^2 & (0 \le |x| \le 1) \\ +\frac{1}{2}|x|^5 - 4|x|^4 + \frac{25}{2}|x|^3 - 19|x|^2 + 14|x| - 4 & (1 \le |x| \le 2) \\ 0 & (2 \le |x|) \end{cases} \tag{B9}$$

Keys' cubic

$$r(x) = \begin{cases} +\frac{4}{3}|x|^3 - \frac{7}{3}|x|^2 + 1 & (0 \le |x| \le 1) \\ -\frac{7}{12}|x|^3 + 3|x|^2 - \frac{59}{12}|x| + \frac{5}{2} & (1 \le |x| \le 2) \\ \frac{1}{12}|x|^3 - \frac{2}{3}|x|^2 + \frac{7}{4}|x| - \frac{3}{2} & (2 \le |x| \le 3) \\ 0 & (3 \le |x|) \end{cases} \tag{B10}$$

BAWA cubic

$$r(x) = \begin{cases} +\frac{1}{2}|x|^3 - |x|^2 - \frac{1}{2}|x| + 1 & (0 \le |x| \le 1) \\ -\frac{1}{6}|x|^3 + |x|^2 - \frac{11}{6}|x| + 1 & (1 \le |x| \le 2) \\ 0 & (2 \le |x|) \end{cases} \tag{B11}$$

Appendix C

Some Analytic Expressions for $\hat{r}(\nu)$ and $e^2(\nu)$

This appendix presents closed form expressions for $\hat{r}(\nu)$ and $e^2(\nu)$ for several interpolants. These formulas were used to validate the numerical procedures used for calculating the values of $\hat{r}(\nu)$ and $e^2(\nu)$ for all interpolants, to confirm the remarkably similar behavior found for PCC and the BAWA cubic below the Nyquist frequency, and to check that the results for exponential and nu splines approach those for linear interpolation in the limit of large tensions. The expressions for linear interpolation and PCC were published previously in references 2 and 3, respectively. The reconstruction filter for the BAWA cubic was given in reference 9. The expression for $e^2(\nu)$ for the BAWA cubic is new. We use the standard definition sinc $(x) = \sin(\pi x)/(\pi x)$.

Linear interpolation

$$\hat{r}(\nu) = \operatorname{sinc}^2(\nu) \tag{C1}$$

$$e^2(\nu) = 1 - 2\hat{r}(\nu) + \frac{2 + \cos(2\pi\nu)}{3} \tag{C2}$$

BAWA cubic

$$\hat{r}(\nu) = \left[1 + \frac{(2\pi\nu)^2}{6}\right] \operatorname{sinc}^4(\nu) \tag{C3}$$

$$e^2(\nu) = \frac{1678}{945} - 2\hat{r}(\nu) + 2\left[\frac{257}{1680}\cos(2\pi\nu) - \frac{3}{70}\cos(4\pi\nu) + \frac{31}{15120}\cos(6\pi\nu)\right] \tag{C4}$$

PCC and cubic Hermite interpolation

$$\hat{r}(\nu) = \hat{r}_0(\nu) + \alpha\hat{r}_1(\nu) \tag{C5}$$

where

$$\left.\begin{aligned} \hat{r}_0(\nu) &= \frac{3}{(\pi\nu)^2}\left[\operatorname{sinc}^2(\nu) - \operatorname{sinc}(2\nu)\right] \\ \hat{r}_1(\nu) &= \frac{2}{(\pi\nu)^2}\left[3\operatorname{sinc}^2(2\nu) - 2\operatorname{sinc}(2\nu) - \operatorname{sinc}(4\nu)\right] \end{aligned}\right\} \tag{C6}$$

and

$$e^2(\nu) = e_0(\nu) - 2\alpha e_1(\nu) + \alpha^2 e_2(\nu) \tag{C7}$$

where

$$\left.\begin{aligned} e_0(\nu) &= 2 - 2\hat{r}_0(\nu) - \frac{18}{35}\sin^2(\pi\nu) \\ e_1(\nu) &= \hat{r}_1(\nu) + \frac{13}{105}\sin^2(2\pi\nu) \\ e_2(\nu) &= \frac{2}{105}\sin^2(2\pi\nu)\left[1 + 6\sin^2(\pi\nu)\right] \end{aligned}\right\} \tag{C8}$$

References

1. De Boor, Carl: *A Practical Guide to Splines.* Springer-Verlag, c.1978.
2. Park, Stephen K.; and Schowengerdt, Robert A.: Image Sampling, Reconstruction, and the Effect of Sample-Scene Phasing. *Appl. Opt.*, vol. 21, no. 17, Sept. 1, 1982, pp. 3142–3151.
3. Park, Stephen K.; and Schowengerdt, Robert A.: Image Reconstruction by Parametric Cubic Convolution. *Comput. Vis., Graph., and Image Process.*, vol. 23, no. 2, Aug. 1983, pp. 258–272.
4. Kochanek, Doris H. U.; and Bartels, Richard H.: Interpolating Splines With Local Tension, Continuity, and Bias Control. *Comput. Graph.*, vol. 18, no. 3, July 1984, pp. 33–41.
5. Cline, Alan K.: Curve Fitting Using Splines Under Tension. *Atmos. Technol.*, Sept. 1973, pp. 60–65.
6. McCartin, B. J.: Applications of Exponential Splines in Computational Fluid Dynamics. *AIAA J.*, vol. 21, no. 8, Aug. 1983, pp. 1059–1065.
7. Nielson, Gregory M.: Rectangular ν-Splines. *IEEE Comput. Graph. and Appl.*, vol. 6, no. 2, Feb. 1986, pp. 35–40.
8. Keys, Robert G.: Cubic Convolution Interpolation for Digital Image Processing. *IEEE Trans. Acoust., Speech, and Signal Process.*, vol. ASSP-29, no. 6, Dec. 1981, pp. 1153–1160.
9. Bolgiano, L. P., Jr.; Abdou, I. E.; Wofford, F. C.; and Amblard, F. G.: A Nondifferentiable Pulse With a More Band-Limited Spectrum Than a Differentiable One. *Proc. IEEE*, vol. 73, no. 1, Jan. 1985, pp. 159–160.
10. McAllister, David F.; and Roulier, John A.: An Algorithm for Computing a Shape-Preserving Osculatory Quadratic Spline. *ACM Trans. Math. Softw.*, vol. 7, no. 3, Sept. 1981, pp. 331–347.
11. Dodd, S. L.; McAllister, D. F.; and Roulier, J. A.: Shape-Preserving Spline Interpolation for Specifying Bivariate Functions on Grids. *IEEE Comput. Graph. and Appl.*, vol. 3, no. 6, Sept. 1983, pp. 70–79.
12. Pratt, William K.: *Digital Image Processing.* John Wiley & Sons, Inc., c.1978.

Table I. Summary of Properties of Interpolants Analyzed

Name	Degree	Type	Control parameters	Order of continuity[a]
Cubic Hermite	3	Local, 4 points	Slope	C^1
Quintic Hermite	5	Local, 4 points	Slope and curvature	C^2
Exponential		Global	Tension	C^2
Cubic spline	3	Global		C^2
Nu spline	3	Global	Tension	C^2
PCC	3	Local, 4 points	Slope	C^1
Keys' cubic	3	Local, 6 points		C^1
BAWA cubic	3	Local, 4 points		C^0

[a]Of both the interpolating and the interpolation functions.

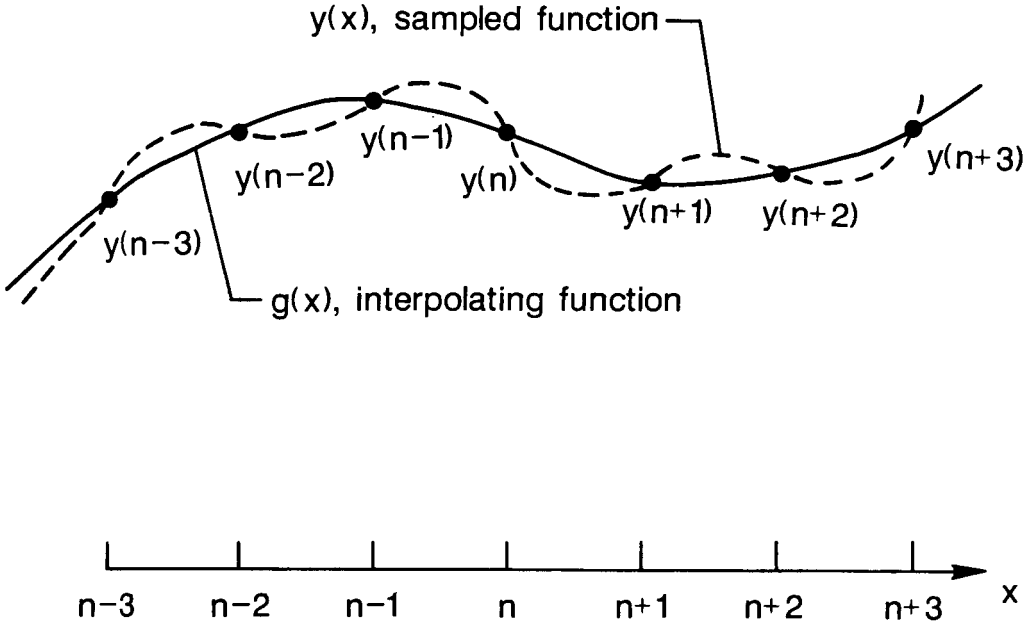

Figure 1. Sampled and interpolating functions.

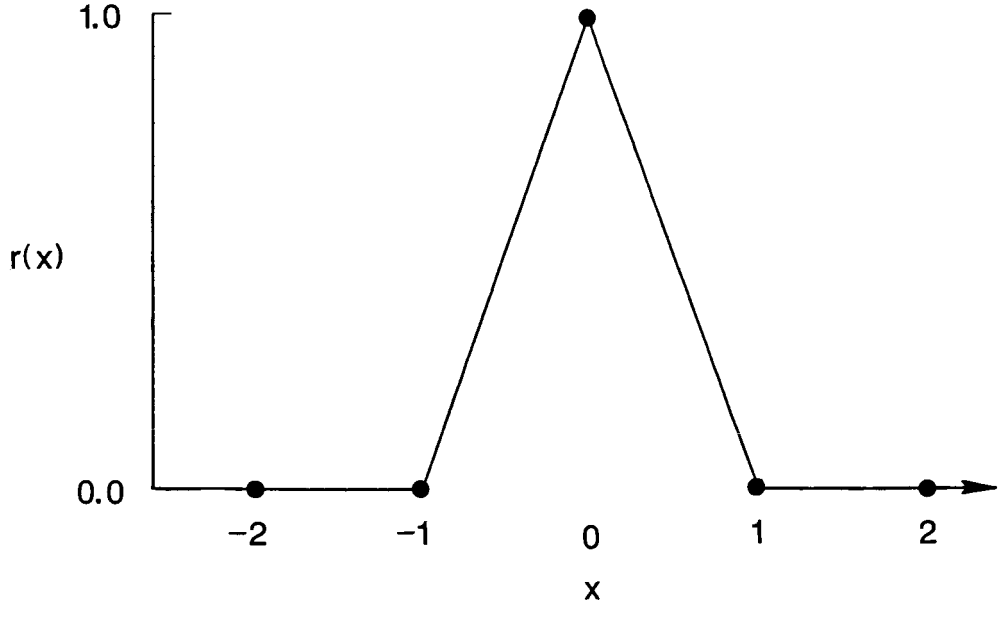

Figure 2. Interpolation function for linear interpolation.

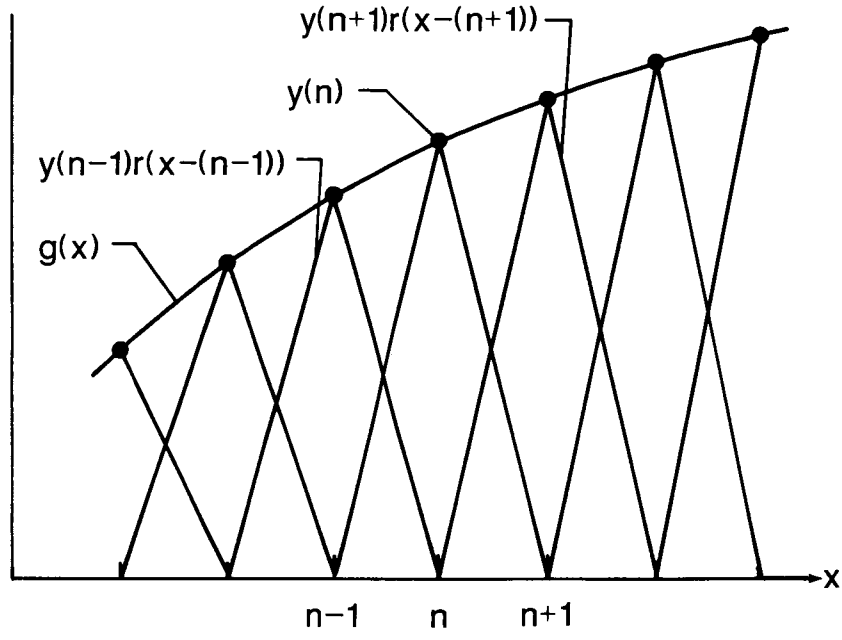

Figure 3. Superposition of linear interpolation functions.

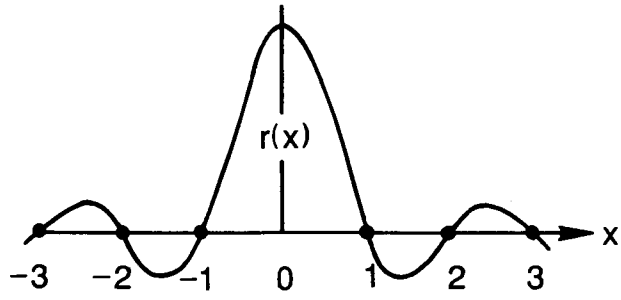

(a) Interpolation function.

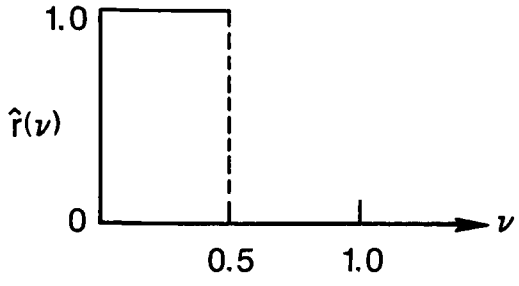

(b) Reconstruction filter.

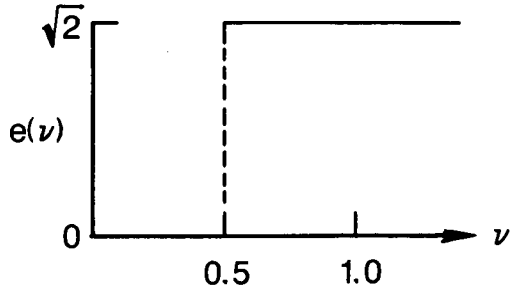

(c) Function $e(\nu)$.

Figure 4. Characteristics of the ideal interpolant.

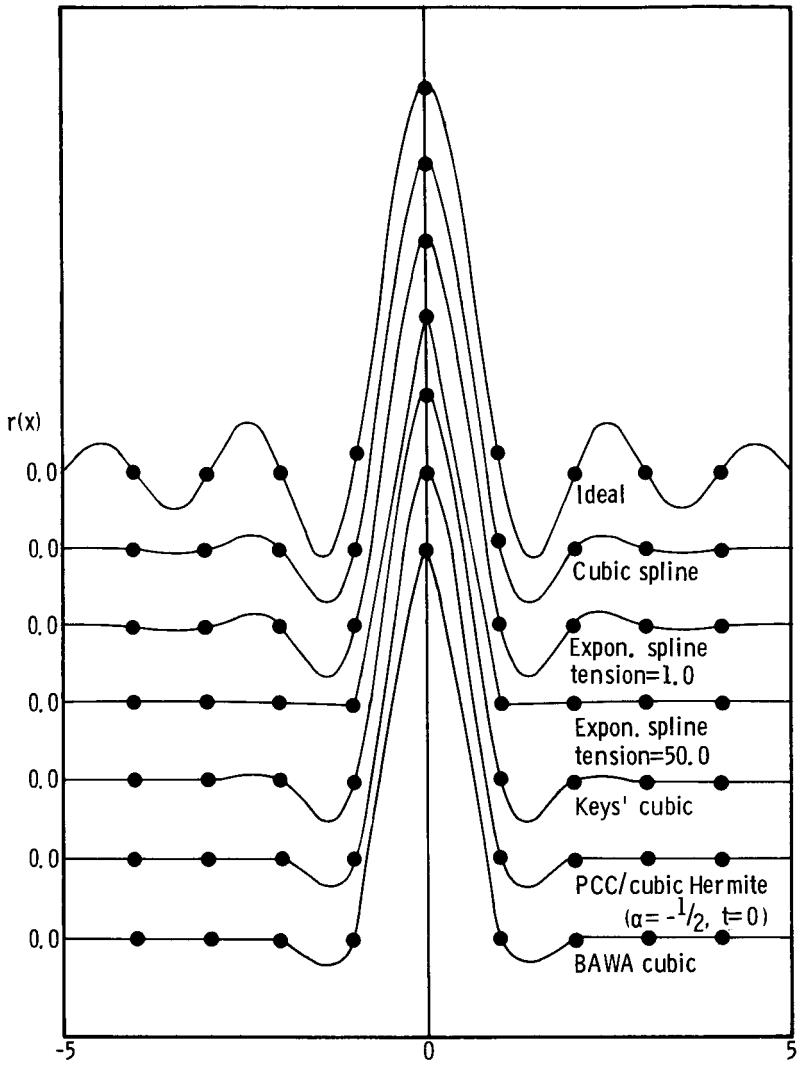

Figure 5. Interpolation functions.

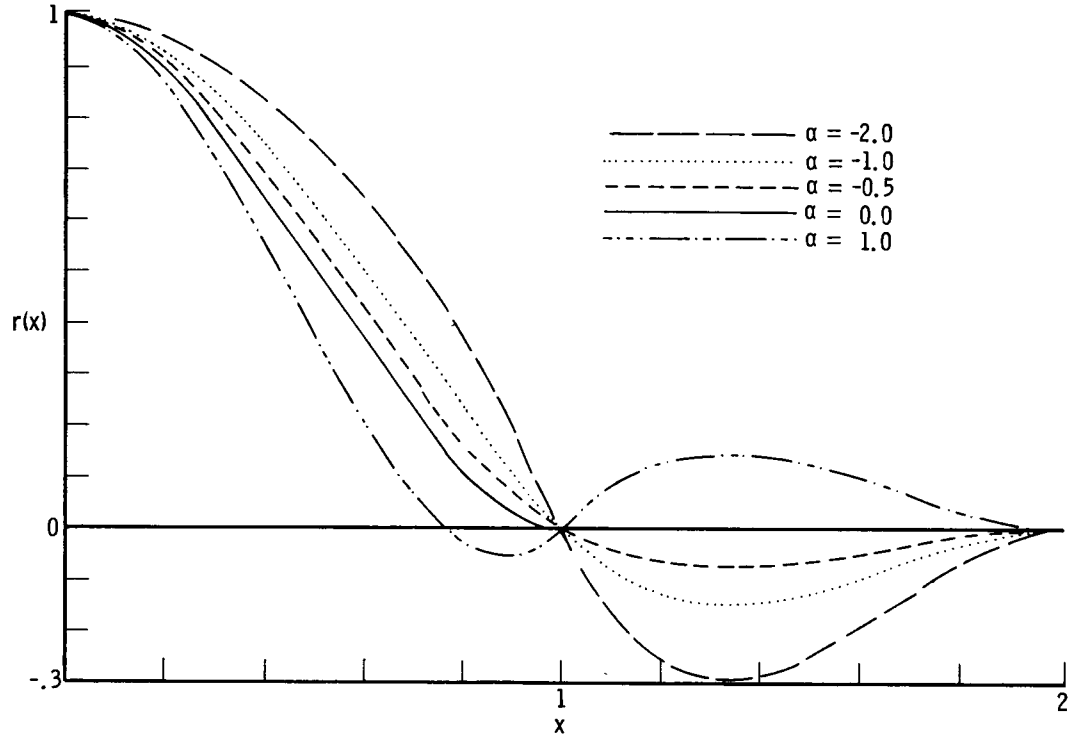

(a) Cubic Hermite and PCC.

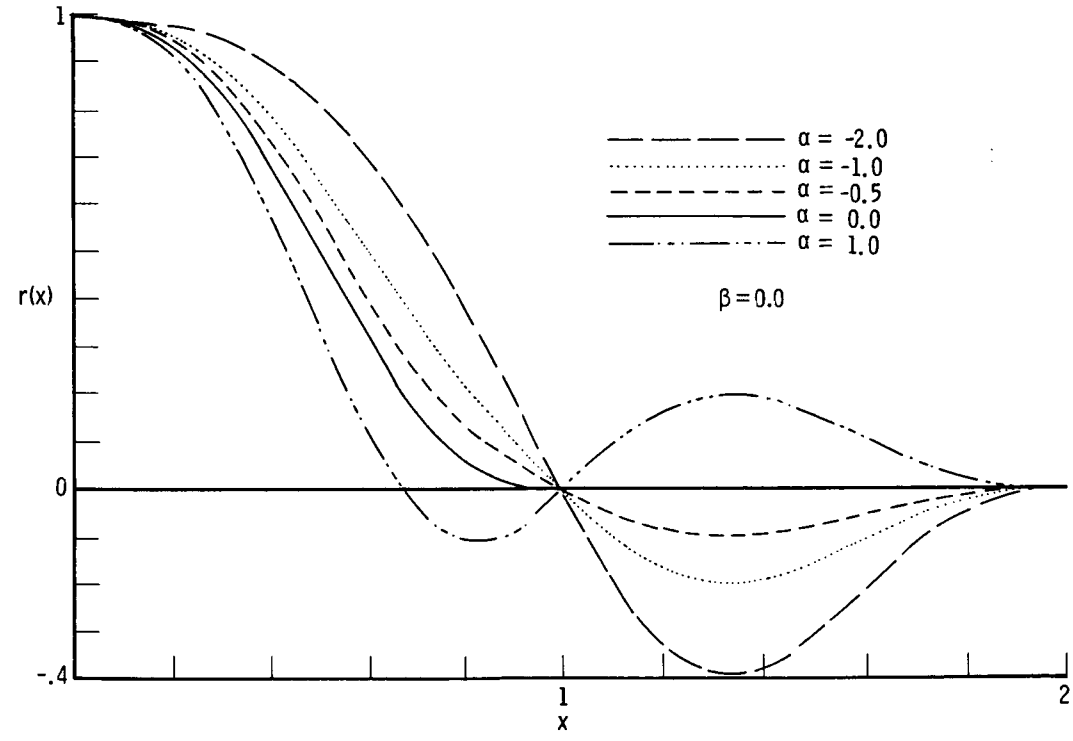

(b) Quintic Hermite.

Figure 6. Interpolation functions for parametric Hermite splines.

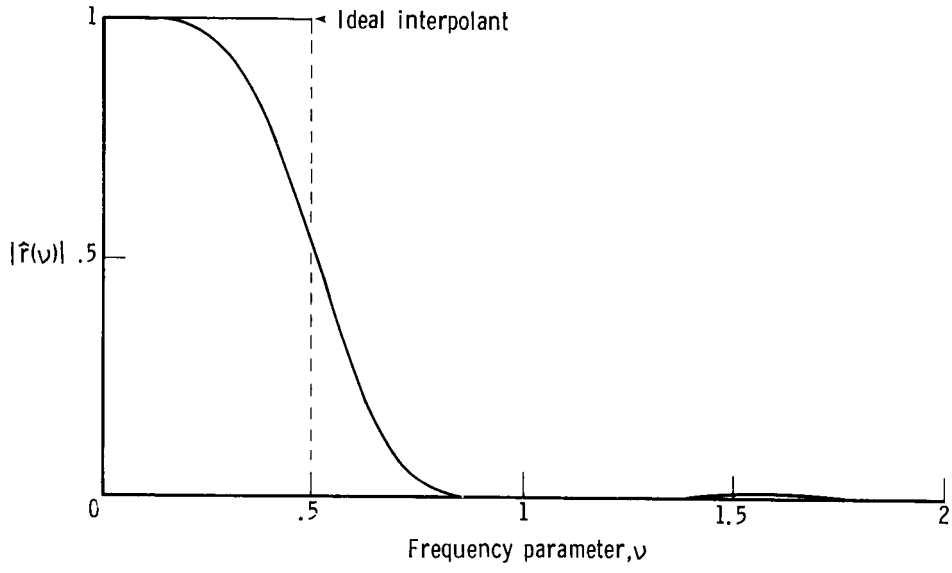

(a) Keys' cubic.

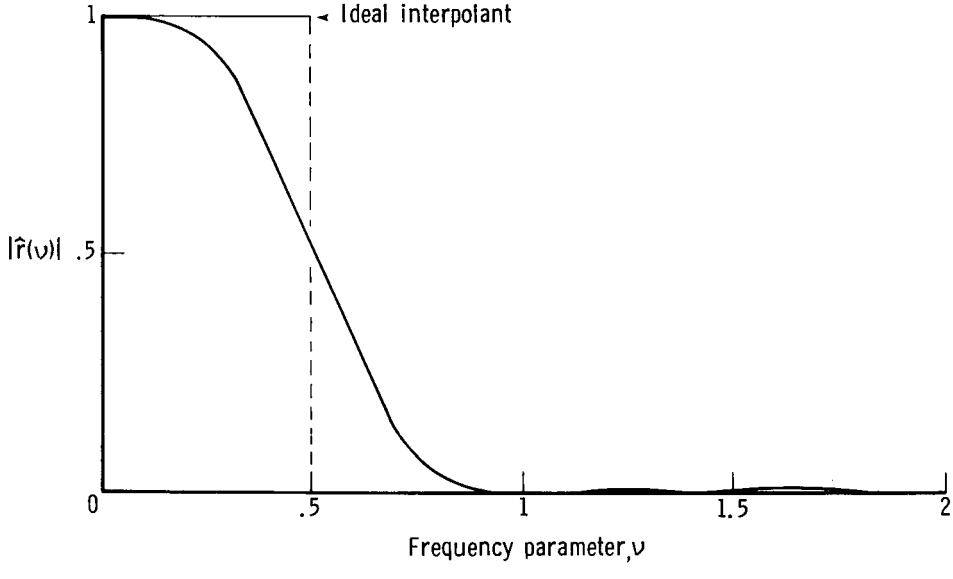

(b) PCC and cubic Hermite, with $\alpha = -1/2,\ t = 0$.

Figure 7. Reconstruction filters.

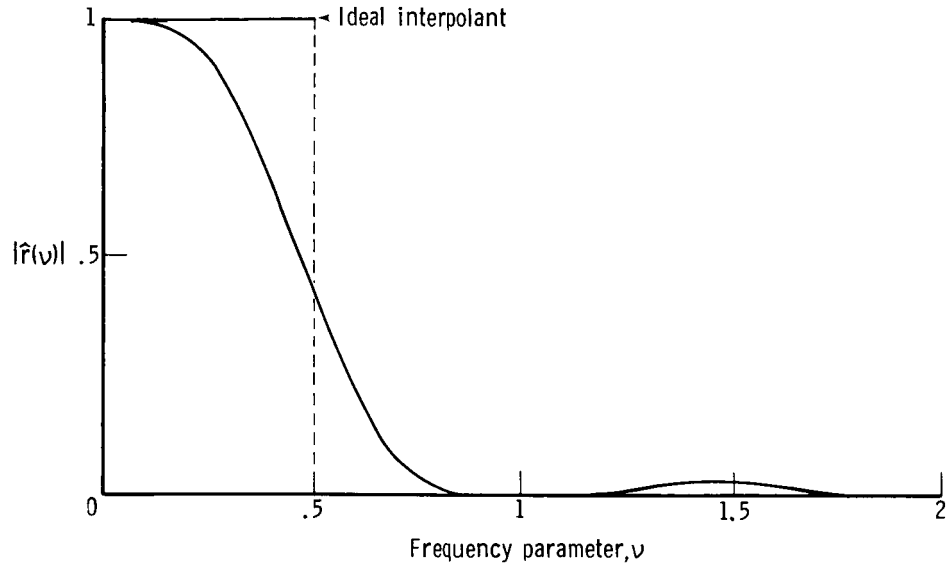

(c) BAWA cubic.

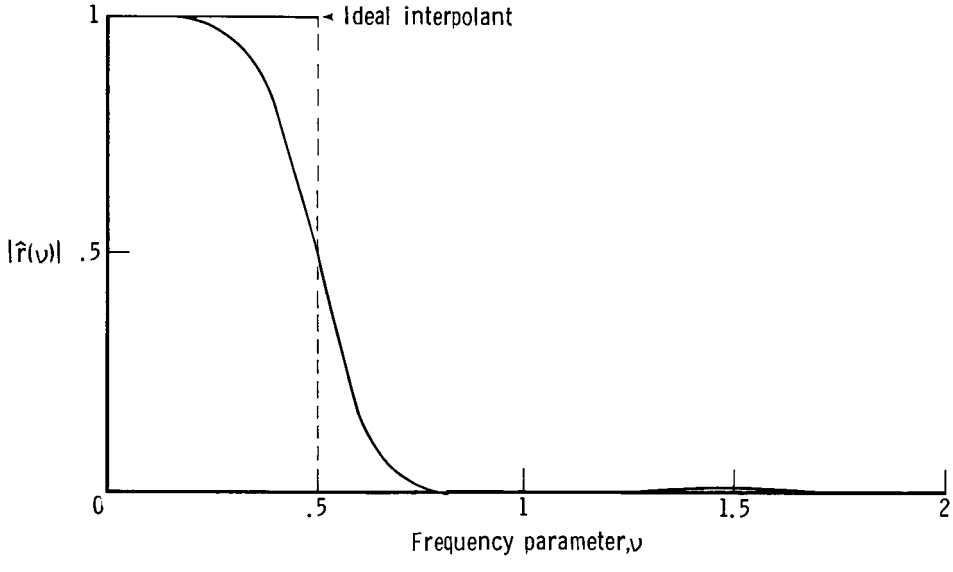

(d) Cubic spline.

Figure 7. Continued.

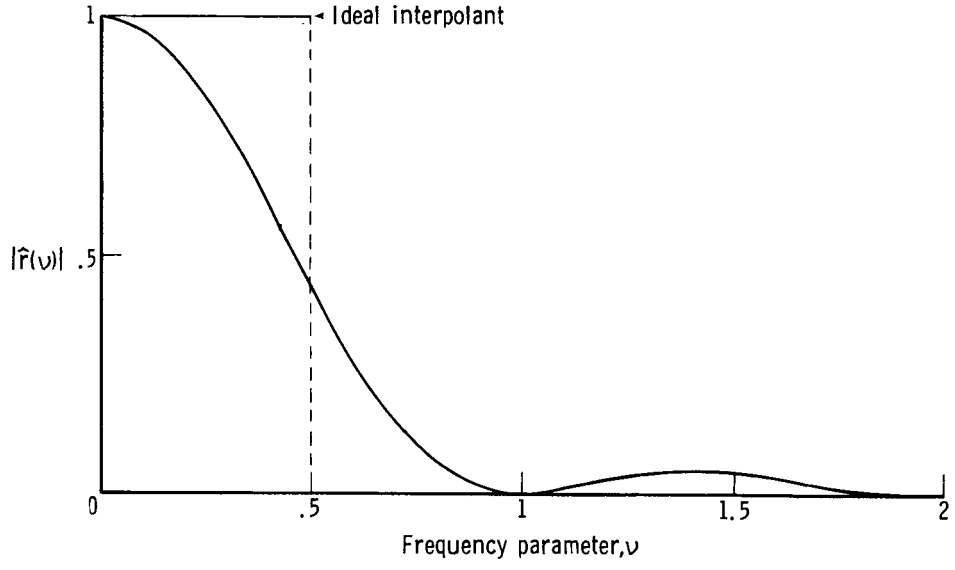

(e) Exponential spline, with Tension = 50.0.

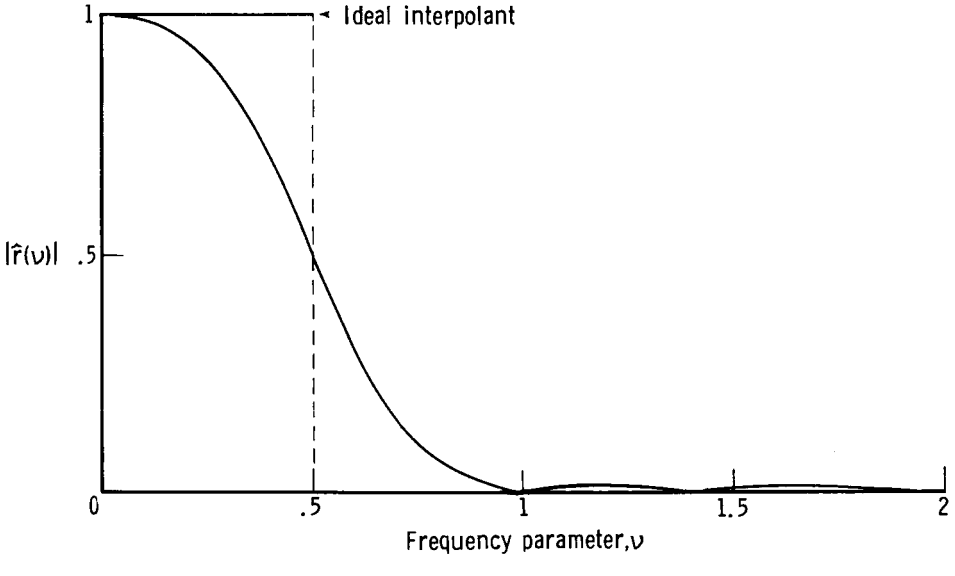

(f) Nu spline, with Tension = 10.0.

Figure 7. Concluded.

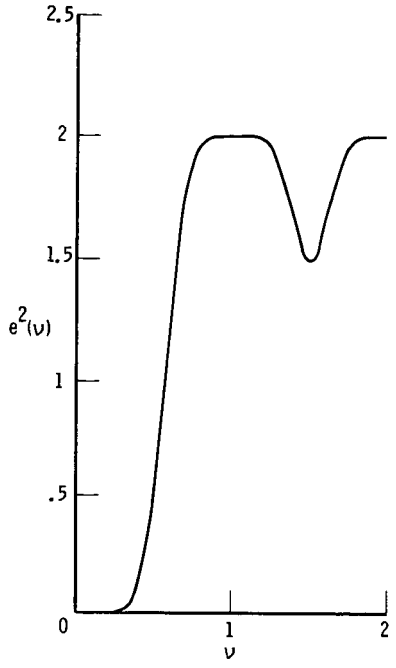

(a) Keys' cubic.

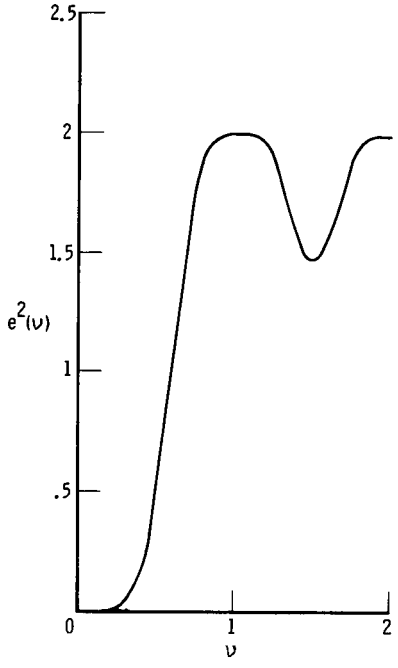

(b) PCC, $\alpha = -1/2$.

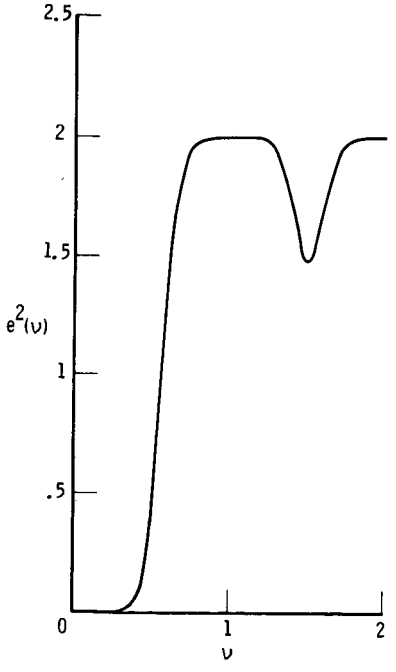

(c) Cubic spline.

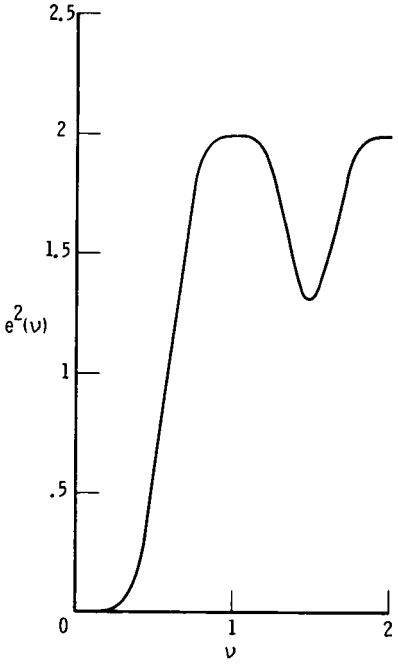

(d) BAWA cubic.

Figure 8. Plots of functions $e^2(\nu)$ for selected interpolants.

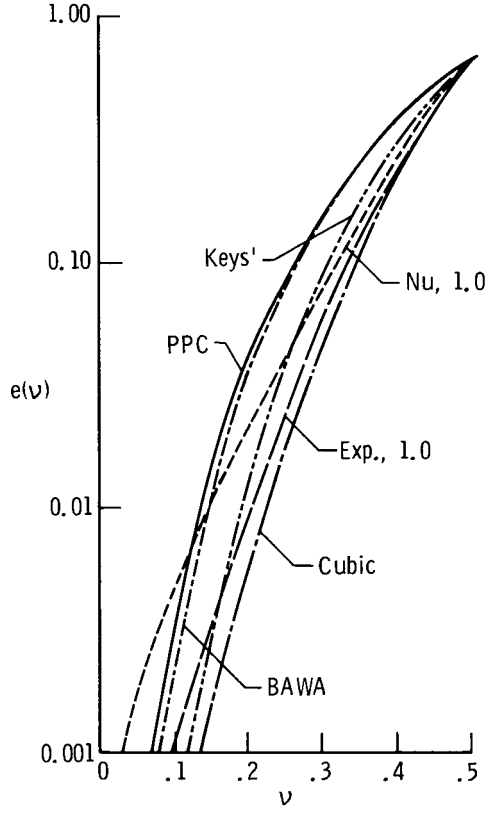

Figure 9. Composite of $e(\nu)$ functions for selected interpolants.

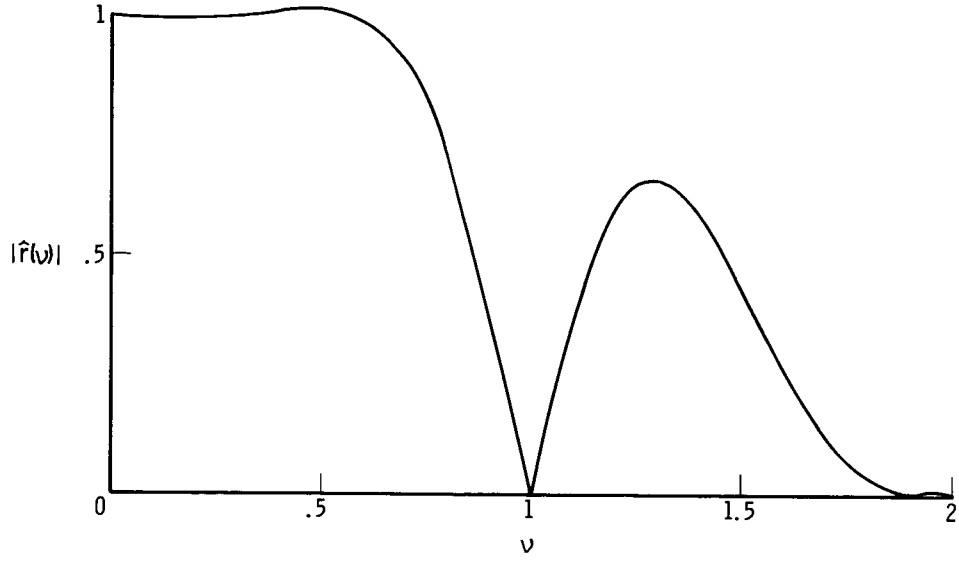

(a) Reconstruction filter.

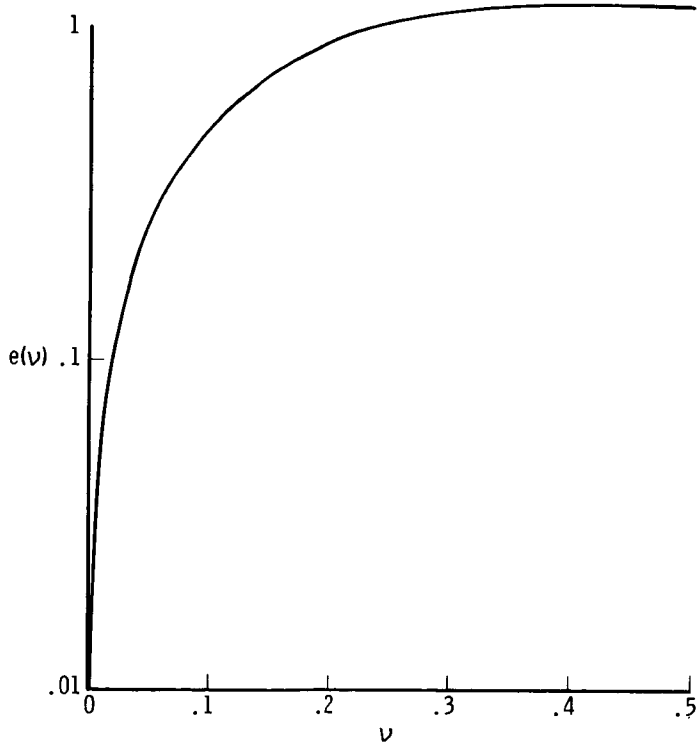

(b) Function $e(\nu)$.

Figure 10. Parametric quintic Hermite spline, with $\alpha = 117/32$, $\beta = 37$.

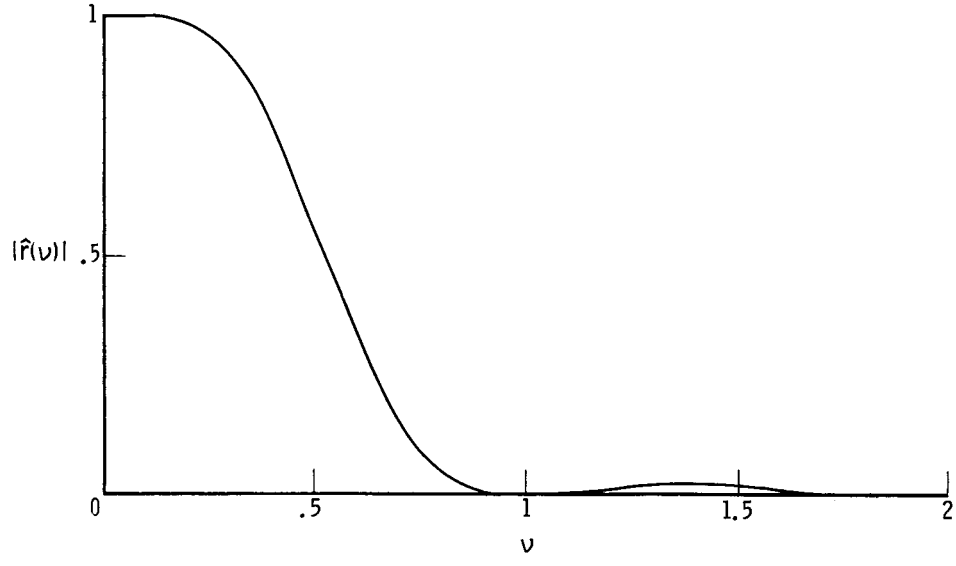

(a) Reconstruction filter.

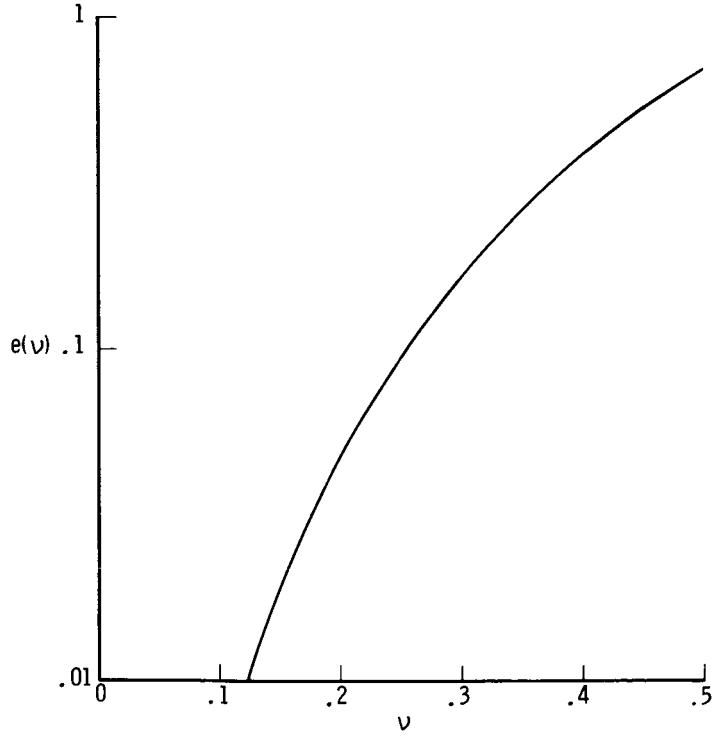

(b) Function $e(\nu)$.

Figure 11. Parametric quintic Hermite spline, with $\alpha = -1/2$, $\beta = -1$.

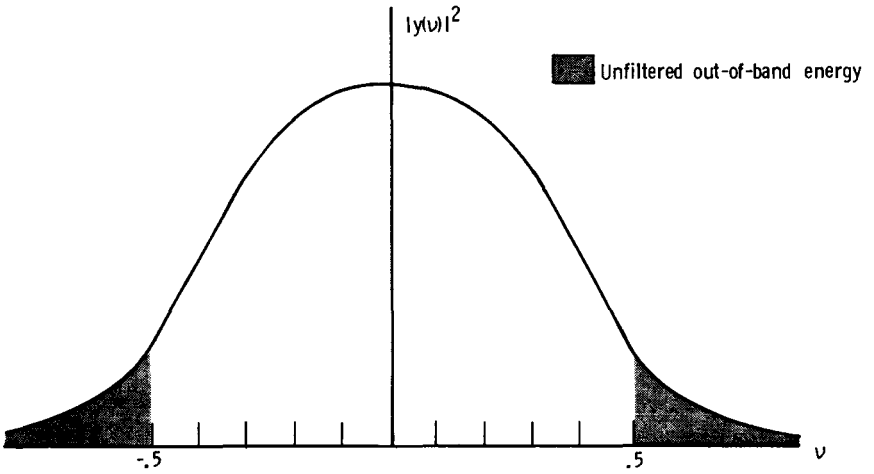

Figure 12. Schematic of unfiltered data energy spectrum.

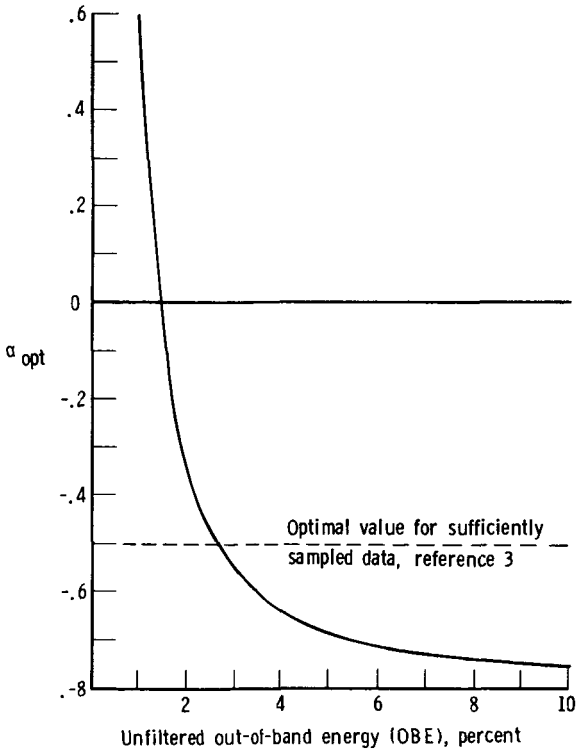

Figure 13. Optimum α for PCC.

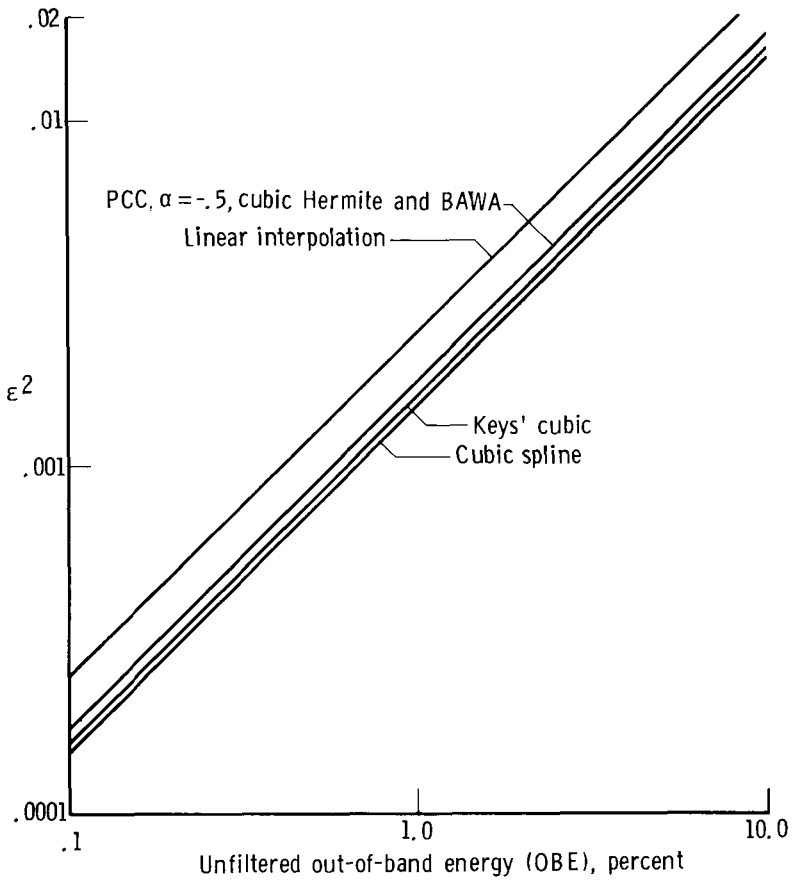

Figure 14. Mean square errors for several interpolants.

NASA
National Aeronautics and Space Administration

Report Documentation Page

1. Report No.	2. Government Accession No.	3. Recipient's Catalog No.
NASA TP-2688		

4. Title and Subtitle	5. Report Date
Quantitative Analysis of the Reconstruction Performance of Interpolants	May 1987
	6. Performing Organization Code
7. Author(s)	8. Performing Organization Report No.
Donald L. Lansing and Stephen K. Park	L-16164
9. Performing Organization Name and Address	10. Work Unit No.
NASA Langley Research Center Hampton, VA 23665-5225	505-60-01-01
	11. Contract or Grant No.
12. Sponsoring Agency Name and Address	13. Type of Report and Period Covered
National Aeronautics and Space Administration Washington, DC 20546-0001	Technical Paper
	14. Sponsoring Agency Code

15. Supplementary Notes

Donald L. Lansing: Langley Research Center, Hampton, Virginia.
Stephen K. Park: The College of William and Mary, Williamsburg, Virginia.

16. Abstract

The analysis presented provides a quantitative measure of the reconstruction or interpolation performance of linear, shift-invariant interpolants. The performance criterion is the mean square error of the difference between the sampled and reconstructed functions. The analysis is applicable to reconstruction algorithms used in image processing and to many types of splines used in numerical analysis and computer graphics. When formulated in the frequency domain, the mean square error clearly separates the contribution of the interpolation method from the contribution of the sampled data. The equations provide a rational basis for selecting an "optimal" interpolant; that is, one which minimizes the mean square error. The analysis has been applied to a selection of frequently used data splines and reconstruction algorithms: parametric cubic and quintic Hermite splines, exponential and nu splines (including the special case of the cubic spline), parametric cubic convolution, Keys' fourth-order cubic, and a cubic with a discontinuous first derivative. The emphasis in this paper is on the image-dependent case in which no a priori knowledge of the frequency spectrum of the sampled function is assumed.

17. Key Words (Suggested by Authors(s))	18. Distribution Statement
Interpolation Splines Reconstruction Image analysis Numerical analysis	Unclassified—Unlimited Subject Category 64

19. Security Classif.(of this report)	20. Security Classif.(of this page)	21. No. of Pages	22. Price
Unclassified	Unclassified	33	A03

NASA-Langley, 1987
For sale by the National Technical Information Service, Springfield, Virginia 22161-2171